Magnetic Resonance Imaging 65 (2020) 15–26

Contents lists available at ScienceDirect

Magnetic Resonance Imaging

journal homepage: www.elsevier.com/locate/mri

Original contribution

STrategically Acquired Gradient Echo (STAGE) imaging, part III: Technical advances and clinical applications of a rapid multi-contrast multi-parametric brain imaging method

E. Mark Haacke[a,b,c,*], Yongsheng Chen[a,d], David Utriainen[b,c], Bo Wu[c], Yu Wang[e,f], Shuang Xia[g], Naying He[h], Chunyan Zhang[i], Xiao Wang[i], M. Marcella Lagana[j], Yu Luo[k], Ali Fatemi[l], Saifeng Liu[b], Sara Gharabaghi[c], Dongmei Wu[e], Sean K. Sethi[a,b,c], Feng Huang[f], Taotao Sun[m], Feifei Qu[a], Brijesh K. Yadav[a], Xiaoyue Ma[n,o], Yan Bai[n,o], Meiyun Wang[n,o,**], Jingliang Cheng[i], Fuhua Yan[h]

[a] Department of Radiology, Wayne State University School of Medicine, Detroit, MI, USA
[b] The MRI Institute for Biomedical Research, Bingham Farms, MI, USA
[c] Magnetic Resonance Innovations, Inc., Bingham Farms, MI, USA
[d] Department of Neurology, Wayne State University School of Medicine, Detroit, MI, USA
[e] Shanghai Key Laboratory of Magnetic Resonance, School of Physics and Electronic Science, East China Normal University, Shanghai, China
[f] Neusoft Medical Systems Co., Ltd., Shanghai, China
[g] Department of Radiology, Tianjin First Central Hospital, Tianjin, China
[h] Department of Radiology, Ruijin Hospital, Shanghai Jiao Tong University School of Medicine, Shanghai, China
[i] Department of MRI, The First Affiliated Hospital of Zhengzhou University, Zhengzhou, China
[j] IRCCS, Fondazione Don Carlo Gnocchi ONLUS, Milano, Italy
[k] Department of Radiology, Translational Research Institute of Brain and Brain-Like Intelligence, Shanghai Fourth People's Hospital Affiliated to Tongji University School of Medicine, Shanghai, China
[l] Departments of Radiology and Radiation Oncology, University of Mississippi Medical Center, Jackson, MS, USA
[m] Department of Radiology, International Peace Maternity and Child Health Hospital, Shanghai Jiao Tong University School of Medicine, Shanghai, China
[n] Department of Radiology, Henan Provincial People's Hospital, Zhengzhou, China
[o] Department of Radiology, Zhengzhou University People's Hospital, Zhengzhou, China

ARTICLE INFO

Keywords:
Quantitative magnetic resonance imaging
Susceptibility weighted imaging
T1 mapping
Quantitative susceptibility mapping
Multi-parametric magnetic resonance imaging
Strategically acquired gradient echo

ABSTRACT

One major thrust in radiology today is image standardization with a focus on rapidly acquired quantitative multi-contrast information. This is critical for multi-center trials, for the collection of big data and for the use of artificial intelligence in evaluating the data. Strategically acquired gradient echo (STAGE) imaging is one such method that can provide 8 qualitative and 7 quantitative pieces of information in 5 min or less at 3 T. STAGE provides qualitative images in the form of proton density weighted images, T1 weighted images, T2* weighted images and simulated double inversion recovery (DIR) images. STAGE also provides quantitative data in the form of proton spin density, T1, T2* and susceptibility maps as well as segmentation of white matter, gray matter and cerebrospinal fluid. STAGE uses vendors' product gradient echo sequences. It can be applied from 0.35 T to 7 T across all manufacturers producing similar results in contrast and quantification of the data. In this paper, we discuss the strengths and weaknesses of STAGE, demonstrate its contrast-to-noise (CNR) behavior relative to a large clinical data set and introduce a few new image contrasts derived from STAGE, including DIR images and a new concept referred to as true susceptibility weighted imaging (tSWI) linked to fluid attenuated inversion recovery (FLAIR) or tSWI-FLAIR for the evaluation of multiple sclerosis lesions. The robustness of STAGE T1 mapping was tested using the NIST/NIH phantom, while the reproducibility was tested by scanning a given individual ten times in one session and the same subject scanned once a week over a 12-week period. Assessment of the CNR for the enhanced T1W image (T1WE) showed a significantly better contrast between gray matter and white matter than conventional T1W images in both patients with Parkinson's disease and healthy controls. We also present some clinical cases using STAGE imaging in patients with stroke, metastasis, multiple sclerosis and a

* Correspondence to: E.M. Haacke, MR Research Core, Harper Hospital, 3990 John R, Detroit, MI 48201, USA.
** Correspondence to: M. Wang, Henan Provincial People's Hospital, Zhengzhou, China.
E-mail addresses: nmrimaging@aol.com (E.M. Haacke), mywang@ha.edu.cn (M. Wang).

https://doi.org/10.1016/j.mri.2019.09.006
Received 16 June 2019; Received in revised form 11 September 2019; Accepted 15 September 2019
0730-725X/ Published by Elsevier Inc.

fetus with ventriculomegaly. Overall, STAGE is a comprehensive protocol that provides the clinician with numerous qualitative and quantitative images.

1. Introduction

A continuing theme over the years in neuroradiology has been the standardization of magnetic resonance imaging (MRI) data for certain diseases such as dementia, multiple sclerosis and stroke. [1–5] This is critical for multi-center trials, for the collection of big data and the use of artificial intelligence in evaluating the data. In the past, there have been attempts to standardize neuro-imaging for neuro-degenerative and neuro-vascular imaging in general but most of these protocols are fairly long in duration. [6–11] A second more recent major effort in the field is rapid, multi-contrast imaging to collect whole brain images in the matter of minutes and provide both qualitative and quantitative images at the same time. [12–17]

Recently, we introduced one such method referred to as strategically acquired gradient echo (STAGE) imaging [18,19] which is designed to establish a standardized, rapid brain imaging method for evaluating neurological diseases. STAGE is a rapid full brain 3D gradient echo (GRE) imaging approach that can be obtained in 4 to 5 (6 to 7.5) min with current clinical 3 T (1.5 T) scanners and can provide similar results for any manufacturer's system thereby providing standardization of brain imaging. Its current clinical applications including cancer, dementia, multiple sclerosis (MS), Parkinson's disease (PD) and stroke are under investigation over several dozen collaborating sites around the world.

In this paper, we 1) discuss the strengths and weaknesses of STAGE; 2) introduce a few new image contrasts and quantifications derived from STAGE, including true proton spin density mapping (tPSD, we use PSD as the abbreviation in this paper rather than the commonly used PD to avoid confusion since PD is commonly used to represent Parkinson's Disease) mapping, synthetic double inversion recovery (sDIR) images and a new concept referred to as true susceptibility weighted imaging (tSWI) linked to fluid-attenuated inversion recovery (FLAIR) or tSWI-FLAIR for the evaluation of MS lesions; 3) demonstrate the contrast-to-noise (CNR) behavior of the T1 weighted enhanced image (T1WE) relative to a large clinical data set; 4) validate the robustness of STAGE T1 mapping using the NIST/NIH phantom, and the reproducibility in a single session versus scanning over multiple sessions on the same subject; and 5) review current clinical results from a number of collaborating sites around the world, including demonstrating the use of STAGE in studying the fetus, stroke, metastases and other neurodegenerative and neurovascular diseases [20,21].

The motivation for introducing tSWI-FLAIR comes from the need to diagnosis white matter hyperintensities (WMH) which requires the use of a T2W imaging protocol. This is particularly important in diseases such as MS to evaluate the presence of WMH in the periventricular space, typically referred to as Dawson's fingers (McDonald Criteria) [22,23]. Acute disruption of the blood brain barrier (BBB) is also evaluated based on the leakage of T1 shortening contrast agents into the brain parenchyma. Disruption of the BBB occurs at the brain capillary level and can create a toxic environment of hypoxia, inflammatory response and progressive demyelination of the white matter [24,25]. The venocentric nature of MS lesions is well documented [26–29] and the visibility of these central veins may be unique to MS [29]. Therefore, an image acquisition which combines a susceptibility component sensitive to venous imaging as well as T2 would be an important diagnostic tool. The latter is best probed using FLAIR [30–33]. FLAIR can help detect iron related changes within the lesion, either creating a ring-like appearance around the bright MS lesions or creating hypo-intensity throughout the lesion [32,34]. This can also be done by combining susceptibility weighted imaging (SWI) with T2 FLAIR images [34–37]. The ability to visualize the microvasculature of MS lesions could give novel information in the development and progression of MS lesions. In this regard, the use of quantitative susceptibility mapping (QSM) in the form of tSWI-FLAIR could improve the visibility of abnormal veins in MS WMH lesions even using shorter echo times.

Relative to its first introduction, we have expanded the output of STAGE to provide radiofrequency (RF) corrected data for 8 qualitative images in the form of proton density weighted (PDW), T1W, T1WE, SWI, tSWI as well as three sDIR images for white matter (WM), gray matter (GM) and cerebrospinal fluid (CSF), and 7 quantitative images in the form of PSD, tPSD, T1, T2* and quantitative susceptibility mapping (QSM) maps as well as the transmit (B_1^+) and receiver (B_1^-) RF field mappings.

2. Material and methods

2.1. STAGE imaging overview

STAGE generates a set of qualitative and quantitative information from a 4 to 5 min data acquisition at 3 T [18,19]. It is a multi-echo, SWI protocol with two different flip angles (FAs). Using two FAs makes it possible to correct the transmit and receiver field effects (both from RF penetration artifacts and from slice profile effects) and to create a spatially uniform estimate of T1 [19,38–42]. Further, by using a special simulation of the signal from GM, WM and CSF, we can create an isointense image, from which the bias field can be calculated to create uniform images for any FA and any set of receiver coils [19]. The original work on STAGE showed errors in the reproducibility of the T1 and PSD maps on the order of 3–5% or less when the scan was repeated in the same setting, although no reproducibility study was done across different imaging sessions [19].

Over and above the original T1W and PDW images, an enhanced T1 weighted image (T1WE) can be constructed by appropriately combining the information from the original two FA scans [18]. From this analysis, using the first echo data, 7 images can be obtained including: PDW, T1W, T1WE, T1 map, T2*W PSD map, as well as the B_1^+ and B_1^- maps. The B_1^+ map can be used to correct the T1 variation from the RF field penetration while the B_1^- map can be used to correct the bias field thereby producing uniform images. Using the second echoes, 5 more image types can be obtained including: T2* maps, SWI, QSM, tSWI and a T2* corrected tPSD map. From the tPSD, T1 and T2* maps, one can obtain three additional synthetic images using double inversion recovery mechanisms, sDIR images for WM, GM and CSF, respectively. Not counting the two RF maps, this provides 13 pieces of qualitative and quantitative information for the clinician from a 5-min protocol at 3 T.

2.2. STAGE data acquisition and the standardized brain imaging protocol

STAGE was designed to use two fully flow compensated multi-echo SWI sequences [43]. The fully flow compensated data allows for both echoes to have minimal motion artifacts from blood flow and also avoid arteries appearing dark in the subsequent SWI images. The echo times were chosen to be in-phase, and the values were chosen for one short echo and one long echo. The specific value of 7.5 ms for the first echo was chosen to make it possible to visualize the middle cerebral artery vessel wall and to allow QSM [20] to be performed to determine the characteristics of any plaque; that is, whether the plaque was calcification or thrombus representing vulnerable plaque. The second echo

was chosen to be long enough to yield a good SWI dataset but minimize large air/tissue field inhomogeneities adjacent to the mid-brain. Also, these values were chosen so that the complex division of the second echo twice by the first echo yielded an effective echo time of only 2.5 ms which can be used easily for point-by-point phase unwrapping [44,45]. The fact that these two echoes are far enough apart and that the first echo is long enough means that a reasonably low bandwidth (BW) could be used to keep the signal-to-noise (SNR) high (BW/pixel = 240 Hz/pixel). A final advantage of keeping the second echo time to a reasonable time is the fact that the repeat time (TR) can be kept short as well to minimize scan time.

The use of a variable flip angle (VFA) method to extract T1 and PSD has been around a long time [38,46]. Part of the problem with this approach is that it is ill-posed unless three FAs are used - one of which must be very high (near 90°) and even then, poor SNR can lead to a poor reconstruction. The use of a constraint can overcome this ill-posed behavior which is why STAGE first segments the WM and then forces an assumed value onto the normal appearing WM so that only two FAs are needed both well under 90°. The choice of what two FAs to use actually comes, in part, from three conditions related to creating new T1 contrast, optimizing SNR and minimizing RF power deposition. [18,40] The choice of 6° and 24° meets these conditions nicely (with one being less than the Ernst angle and one greater than the Ernst angle for most tissues of interest) with a TR of 25 ms at 3 T. Although slightly different flip angles were used relative to the optimal flip angles, the difference in SNR between these two choices and the optimal choice is small (on the order of 10 to 20%). Too large a FA will lead to more time-of-flight in-flow effects and more pulsatility artifacts which we try to avoid by keeping the second FA reasonably small yet still easily meeting the condition that it be larger than the Ernst angle. The short echo also provides for the best pseudo spin density estimates. Nevertheless, at 7.5 ms there will be remnant T2* effects and dephasing by the air/tissue (sinus/brain) boundaries from 2 mm thick slices. This dephasing can be dramatically reduced by using either thinner slices or reducing the echo time to 5 ms with flow compensation in readout and partition directions but not in the phase encoding direction. If necessary, one can reduce this even further to roughly 2.5 ms by removing flow compensation to effectively eliminate dephasing artifacts. This depends solely on the desired use of the STAGE data and whether the longer first echo time is useful or not for certain types of contrast [43]. The image resolution was chosen to be 0.67 (readout) × 1.34 (phase) × 2.0 (partition) mm^3 specifically for axial coverage for most neuro-imaging. This is already better than what most sites run in that it provides 3D reformattable images because of the reasonably thin slice thickness. The original work was based on the adapted gradient-recalled echo (GRE) sequence to provide full flow compensation for each echo [43]. Typically, commercial GRE sequences only have the ability to do full flow compensation on the first echo, but not second and consequent echoes. Nevertheless, STAGE can be run at any field strength (to date this has been done from 0.35 T to 7 T) and on any manufacturer's scanner with or without full flow compensation.

2.3. The corrections of RF field variations and T1 mapping

There are two spatial variations from RF fields, one from the transmit (B_1^+ or B_{1t}) field and one from the receive field (B_1^- or B_{1r}). The measured signal or magnitude image from a GRE scan is proportional to the product of B_{1r} and the transverse magnetization which is a function of B_{1t}. For 3 T and higher field strengths, the RF transmit field variation is significant and needs to be accounted for when doing quantitative MRI such as T1 and PSD mapping using the VFA method. To date, various efforts have been made in mapping the B1 fields [42,47–53]. STAGE uses two magnitude images acquired with a pair of optimal FAs for mapping brain tissues' longitudinal relaxation [19,40]. The apparent T1 derived from a linear fitting of VFA images is scaled by k^2, where k is the position-related factor representing the B_{1t} variation across the object being imaged. Assuming the entire brain volume has one given T1, a pseudo k map can be easily calculated but it only gives correct values for those voxels having a T1 close to the given value. With a proper segmentation of GM and WM for the entire brain volume, a discrete k map can be generated by combining the two pseudo k maps for GM and WM, which were computed by dividing the T1 reference values for GM and WM from the segmented apparent T1 map [19]. Since the B_{1t} field has a parabolic characterization and a low spatial frequency, we use a local quadratic fitting to estimate the entire k map in a pixel by pixel manner. The fitted k map is then used to extract the B_{1t} corrected T1 map. The effective PSD map (without a correction for T2*) derived from the intercept of the fitted line of signal versus FA, is then scaled by the *bias field*, which is the residual B_{1r} variation. STAGE employs a synthetic image, which was designed to have isointense signal intensity for GM and WM, for fitting and correcting the *bias*. The accuracy of the discrete k maps depends on the accuracy of the brain segmentation. STAGE uses a high pass filter on the WM pseudo k map to segment WM and GM regions by thresholds. A more accurate segmentation from the synthetic DIR images could be used for an iterative solution to this k-map approximation.

2.4. True-PSD map

The PSD map derived from the linear fitting of two or more FAs contains T2* decay via:

$$\rho_i = \rho_0 * e^{-TE_i/T2^*} \quad (1)$$

where ρ_0 is the true PSD (tPSD) map and ρ_i is the PSD map from the linear fitting of each echo. To generate ρ_0, the T2* signal decay should accounted for no matter how short the echo time. This can be accomplished with the dual-echo STAGE data, by calculating T2* from the signal decay between the two PSD maps from each echo.

2.5. STAGE T1 mapping: simulations and phantom study

To maximize T1 accuracy, generally three or more FAs are required: one near the Ernst angle for maximum SNR; and one on each side of the Ernst angle with a signal intensity of the first FA roughly 50 to 70% of that at the Ernst angle and of the second FA rough double the Ernst angle. [40] Therefore, to quantify a smaller T1 (say < 100 ms) one needs to acquire data with a very large FA which is usually impractical at high fields due to specific absorption rate limitations. Likewise, to quantify a larger T1 (say larger than 2000 ms) one needs to collect data with a very low FA which has low SNR.

To evaluate the accuracy and precision of STAGE T1 and PSD mapping, we simulated the T1 and PSD errors given the two selected FAs (6° and 24°) at the given minimal TR (25 ms) used in 3 T in vivo data acquisition and the SNR of the two images estimated from previous in vivo data at 3 T. The well-known spoiled GRE signal equation as a function of flip angle was used for the simulation. A range of T1 from 400 to 3000 ms and PSD from 1% to 100% were used. TE was assumed to be much less than the tissue T2* values. Neither RF field variation was included in the simulation. The SNR of the two simulated images were 35:1 and 45:1 for the 6° and 24° magnitude images (these numbers came from the actual STAGE in vivo data from the genu of corpus callosum). We also did an in vitro study on the ISMRM/NIST standard phantom with known T1 and PSD values for multiple spheres at different locations. 3D GRE data was acquired on a 3 T system (Siemens, Verio) with a 32-channel head coil with the following imaging parameters: TR = 15 ms, TE = 7.5 ms, BW = 170 Hz/pixel, FOV = 256 × 256 mm^2, matrix = 512 × 256, slice thickness = 1.0 mm, in-plane spatial resolution of 0.5 (readout) × 1.0 (phase) mm^2, using FAs of 2°, 4°, 6°, 24° and 45°, respectively, The number of slices collected was 176, with a parallel imaging acceleration factor of 2, and a scan time of 5 min and 9 s for each FA. The reference

T1 value of the background water used for fitting the B1 variations was 3.2 s. A 16 × 16 high-pass filter was used on the first estimated k-map for background segmentation of the material outside the spheres followed by a local quadratic fitting to find the B1 field variation. T1 and PSD values were then re-calculated with the estimated B_{1r} and B_{1t} field variation factor for each voxel. Apparent T1/PSD values (uncorrected) and STAGE T1/PSD (corrected) were compared on the center slice of each plate for those spheres with T1 s ranging from 100 ms to 2000 ms, and PSDs from 20% to 90%, by manually drawing the sphere ROIs.

2.6. In vivo reproducibility of STAGE T1 mapping

In order to test the reproducibility of STAGE, one subject was acquired on two 3 T MRI scanners (A: a Siemens Verio; and B: a Siemens Prisma). The same subject was acquired during 12 different days on scanner A and two different days on scanner B. Moreover, 10 different acquisitions were performed in a row during one of the MRI sessions performed on scanner A, leading to a total of 23 STAGE datasets. T1W images were segmented using the FMRIB's Software Library (FSL, http://www.fmrib.ox.ac.uk/fsl) toolboxes. Deep GM structures (e.g., caudate nucleus (CN); putamen (Put); thalamus (Thal); globus pallidus (GP)) were segmented using the FIRST toolbox [54]. The CSF, WM and cortex were segmented from the T1W image with Sienax [55], after the non-brain tissue removal using the Brain Extraction Toolbox [56]. The CSF, WM, cortical and subcortical GM masks were eroded in order to reduce partial volume effects [57] and used to obtain the median T1 relaxation time in the structures of interest from the T1 map. The average, standard deviation (SD), and the coefficient of variation (CoV = SD / average) were computed for the values obtained from the different runs of the same subject. The CoV was computed separately for the evaluation of repeatability for the continuous runs without re-localization and acquired on different days.

2.7. Simulated DIR images

The concept of DIR requires two inversion pulses separated in time to null two tissues. As such for a three-tissue system (such as the brain with WM, GM and CSF), to acquire an image with just one tissue type would require running the DIR scan three times. This is too long to be practical but once the tissue properties are known, the DIR can be simulated. The goal is to find the appropriate two inversion times to null two of the tissues and leave an image of just one tissue type. As originally presented by Redpath and Smith [58], the second inversion time (TI_2) can be described as a function of a given first TI (TI_1) for nulling a certain tissue of the brain as given in Eq. (2). With known T1 and PSD values from STAGE, the sDIR images for GM, WM and CSF can be found from Eq. (3):

$$TI_2 = -T1 * \ln\left(\frac{E_c - 1}{2E_1 - 1}\right) \quad (2)$$

$$sDIR = -\rho_0 * (1 - 2E_2 + 2E_1E_2 - E_c) \quad (3)$$

where $E_1 = e^{-TI_1/T1}$, $E_2 = e^{-TI_2/T1}$ and $E_c = e^{-TR/T1}$. In this way, the DIR results can be simulated for any given set of imaging parameters and three tissue types.

2.8. Clinical data

Compared to conventional imaging, STAGE offers both T1 and PSD weighted imaging. Even without considering the T2* map, QSM map and SWI data, STAGE already offers more information and saves time over conventional neuroimaging approaches. One question is: "How does the image quality and contrast of STAGE fare against MP-RAGE for example?" To address this question, 67 healthy control (HC) cases and 67 Parkinson's disease patients were measured for CNR and were reviewed by three radiologists each with more than five-year experience in neuroradiology. CNR was measured between the WM and GM for the PUT, CN and cortex. This was done by measuring an ROI in one of the deep gray matter (DGM) or cortical GM regions and in an adjacent WM region. Other representative clinical data were also acquired in patients with stroke, MS, and metastases, and for imaging the fetal brain. For MS cases, the tSWI image was combined with FLAIR images to visualize penetrating veins in WMH lesions.

3. Results

STAGE imaging parameter recommendations for 1.5 T and 3 T systems are given in Table 1. Adding T2 weighted FLAIR and diffusion weighted imaging (DWI) acquisitions, this full brain imaging protocol can be acquired in < 10 min at 3 T. A representative STAGE case acquired at 3 T in 5 min on a healthy volunteer is shown in Fig. 1 compared with the conventional MRI acquired in 5.5 min. Representative tPSD maps are shown in Fig. 2. On the tPSD map, the putamen and globus pallidus were shown to have similar water content while there remained significant signal differences on the incorrected PSD map.

For a given set of imaging parameters and SNR one can simulate the expected errors in T1 and PSD. We found that the errors for WM (T1 = 900 ms, PSD = 70%) and GM (T1 = 1600 ms, PSD = 84%) were 4.79% and 4.83% for T1 (Fig. 3a) and 2.94% and 3.35% for PSD (Fig. 3b).

The ISMRM/NIST Phantom T1 mapping results are shown in Fig. 4. Note that, plate #5 is at the edge of the phantom, plate #4 is at the center of the phantom and plate #3 is near the center of the phantom. Measured PSD values were normalized by setting the largest PSD sphere to be 100% water. The measured errors ($T1_{err}$, PSD_{err}) for STAGE T1 and PSD and those of the apparent values without B1 correction were calculated from the difference between the measured mean ($T1_{mm}$) value and the reference value ($T1_r$) divided by the reference value given by $T1_{err} = (T1_{mm}\text{-}T1_r)/T1_r*100$. STAGE had a 4.5% error for T1 spheres with a value close to that of WM value, a 5.6% error with a

Table 1
STAGE imaging parameters for 3 T (1.5 T).

	Dual-echo version		Single-echo version		
	Scan #1	Scan #2	Scan #1	Scan #2	Scan #3
Sequence	3D GRE	3D GRE	3D GRE	3D GRE	3D GRE
TR (ms)	25 (45)	25 (45)	25 (45)	25 (45)	25 (45)
TEs (ms)	7.5, 17.5 (10, 37)	8.75, 18.75 (10, 37)	7.5 (10)	17.5 (37)	8.75 (10)
Flip angle (deg)	6 (7)	24 (35)	6 (7)	6 (7)	24 (35)
Bandwidth (Hz/pixel)	240 (210)	240 (210)	240 (210)	240 (210)	240 (210)
Slice Thickness (mm)	2.0 (2.7)	2.0 (2.7)	2.0 (2.7)	2.0 (2.7)	2.0 (2.7)
FOV (mm)	256 × 192	256 × 192	256 × 192	256 × 192	256 × 192
Matrix	384 × 144	384 × 144	384 × 144	384 × 144	384 × 144
GRAPPA Acc. Factor	2	2	2	2	2
Scan time (min: *sec*)	2:29 (3:29)	2:29 (3:29)	2:29 (3:29)	2:29 (3:29)	2:29 (3:29)

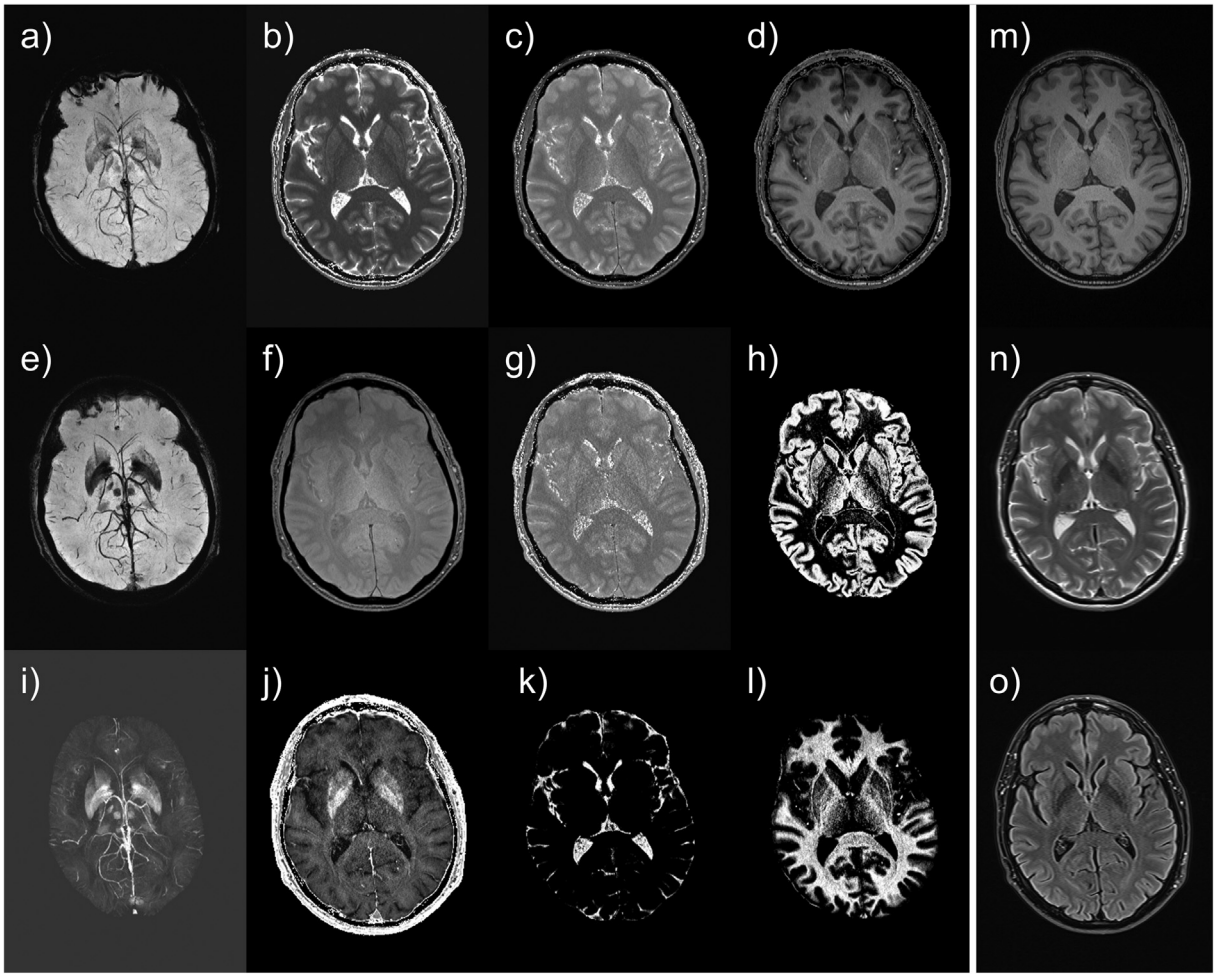

Fig. 1. Comparison between STAGE and conventional MRI on a 67-year old male healthy control subject scanned with the double-echo version of STAGE on a 3 T scanner. Images in the left panel (a-l) were from STAGE taking 5 min with a spatial resolution of $0.67 \times 1.34 \times 2.0\,mm^3$ and 64 slices covering the whole brain. Images in the right panel (m-o) were from conventional MRI providing only T1, T2 and FLAIR in 5.5 min with the same resolution and coverage. a) SWI; b) T1 map; c) PSD map; d) T1WE; e) tSWI; f) PDW; g) tPSD map; h) sDIR-GM; i) QSM; j) R2* map; k) sDIR-CSF; l) sDIR-WM; m) T1-MPRAGE; n) T2 TSE; o) T2 FLAIR. The images for SWI, tSWI and QSM were minimum/maximum intensity projections with an effective slice thickness of 16 mm.

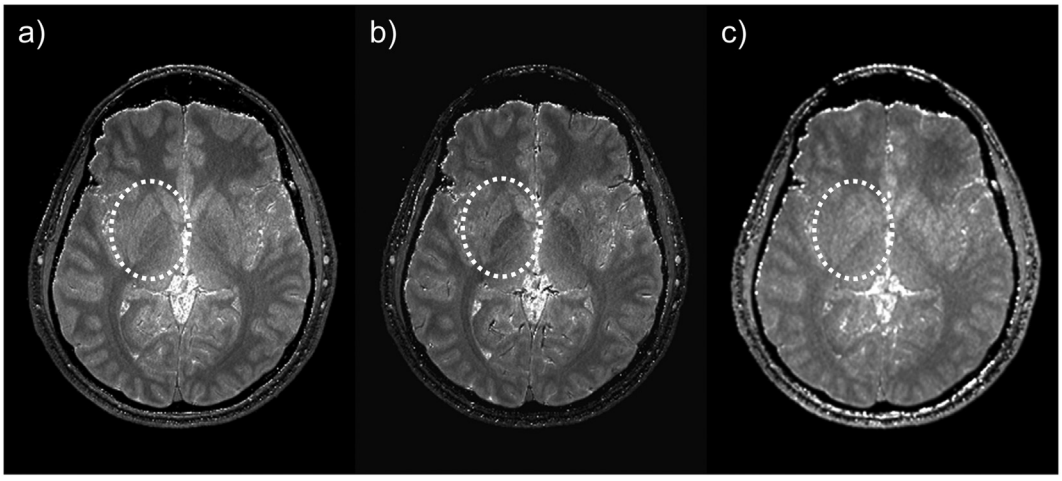

Fig. 2. T2* corrected tPSD map derived from the double-echo STAGE data. a) T2*W-PSD map from the first echo; b) T2*W-PSD map from the second echo; and c) tPSD map. With the T2* decay correction, the tPSD map calculated from the first echo represents pure water content which shows identical proton spin density for caudate nucleus, putamen and globus pallidus, while they are T2* biased on the uncorrected PSD maps (white circle).

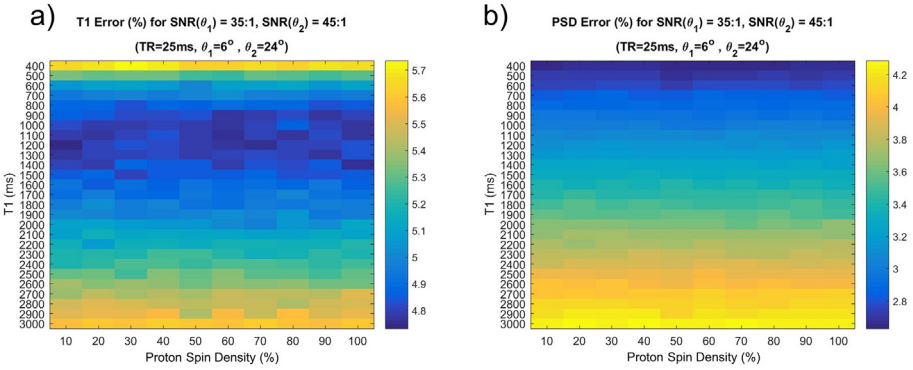

Fig. 3. Simulations for T1 and PSD errors in the VFA method using two-point GRE data and given SNRs assumed from in vivo data for the two magnitude images. The T1 and PSD estimation errors for WM (T1 = 900 ms, PSD = 70%) and GM (T1 = 1600 ms, PSD = 84%) were 4.79% and 4.83% (Fig. 3a) and the PSD errors for WM and GM were 2.94% and 3.35% (Fig. 3b), respectively.

value close to that of GM and a 2.6% average error inclusive of all PSD spheres from 20% to 90% proton density relative to water. Note that the T1 errors were estimated from plate #5 which is at the edge of the phantom.

In vivo results for the estimation of STAGE T1 mapping reproducibility are shown in Fig. 5. For all acquisitions (N = 23), CoV of WM, cortex, Thal, CN, Put and GP were 1.4%, 3.4%, 5.8%, 3.7%, 4.3% and 5.2%, respectively. For the subject data acquired ten times in the same session without repositioning, the CoV of those structures were 0.1%, 0.3%, 1.7%, 1.1%, 1.0%, and 1.3%, respectively. The measures obtained from the same subject acquired multiple times during the same day had lower CoV than those acquired from different days.

For the DIR simulations, the values of TI_1 and TI_2 can be found from the three intersection points shown in Fig. 6. These yield the TI_1 and TI_2 pairs as (1850 ms, 510 ms), (3800 ms, 610 ms) and (4420 ms, 1000 ms) to create images for either CSF, GM and WM alone, respectively, using the following parameters at 3 T: $T1_{WM}$ = 900 ms, $T1_{GM}$ = 1600 ms, $T1_{CSF}$ = 4500 ms, TR = 20 s, PD_{WM} = 0.68, PD_{GM} = 0.84, and PD_{CSF} = 1.0. [59] Representative sDIR images from STAGE data generated using Eq. (3) on a healthy subject are shown in Fig. 7. The three sDIR images can be easily turned into a binary mask to segment GM, WM and CSF in any of the multitude of STAGE images. One example application of simulated DIR images is to present distinct images for GM, WM and CSF without requiring segmentation; they are naturally segmented by this process (Fig. 7).

For the CN, PUT and the cortical GM, the T1WE images of STAGE were superior to both the T1W images of STAGE and MP-RAGE (Fig. 8). For the cortical GM, the contrasts for STAGE T1W and MP-RAGE were not statistically different. The radiologists also rated the image quality on a 5-point scale and determined that, apart from the artifacts in the

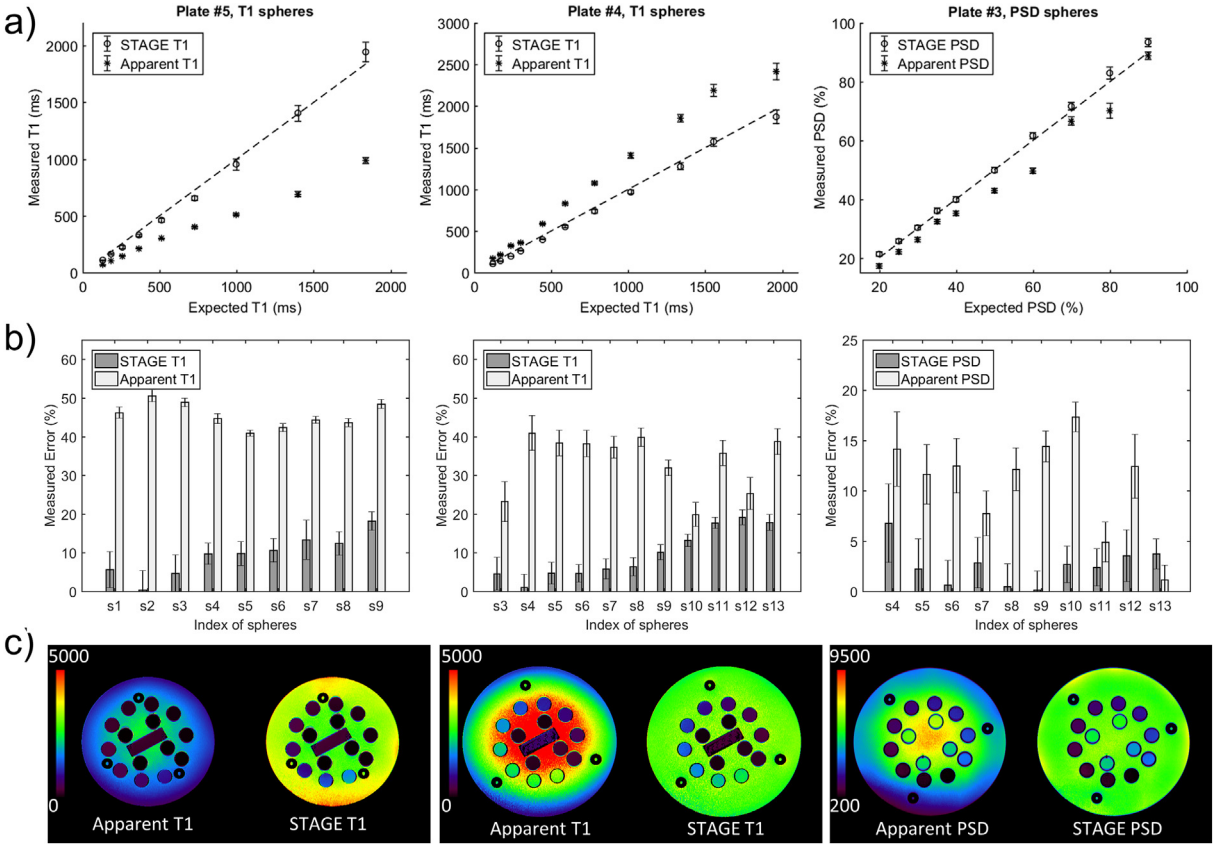

Fig. 4. In vitro validation of STAGE T1/PSD mapping using the ISMRM/NIST standard T1/PSD phantom. a) STAGE T1/PSD, apparent T1/PSD compared with reference values for each plate; b) measured bias (error relative to the reference value for each sphere); and c) apparent and STAGE T1/PSD for the center slice of each plate. STAGE had a 4.5% error for T1 spheres close to WM value, a 5.6% error for the sphere with a value close to GM, and a 2.6% error for all PSD spheres from 20% to 90% proton density relative to water.

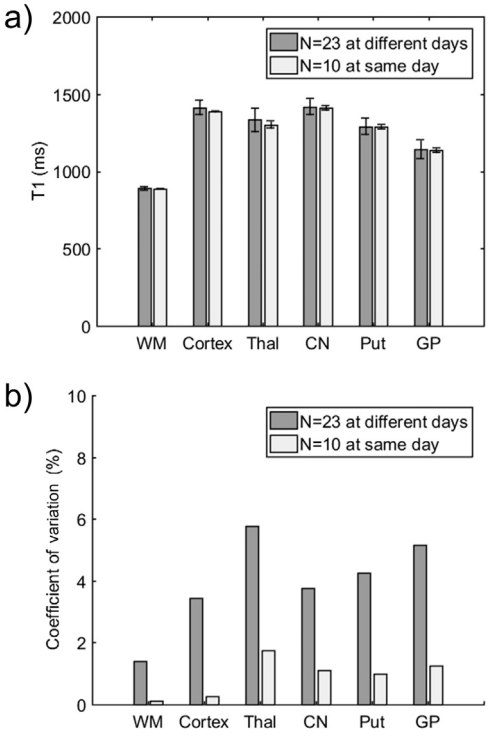

Fig. 5. In vivo reproducibility of STAGE T1 mapping. a) Measured T1 values for each structure; b) Coefficient of variation for each structure. The data from the first group ($N = 23$) were all data acquired on the same subject from two 3 T MRI scanners during 12 different days across two years. The data from the second group ($N = 10$) were collected on the same subject who was scanned ten times sequentially without re-positioning during one sitting. The first group results represent systematic variation from scan/rescan (including variations in position and partial volume effects) superimposed on the statistical variation from the SNR in each image. The second group results represent the error without repositioning and assuming no significant motion and, therefore, represents the inherent SNR of the method itself in the presence of noise in the original images.

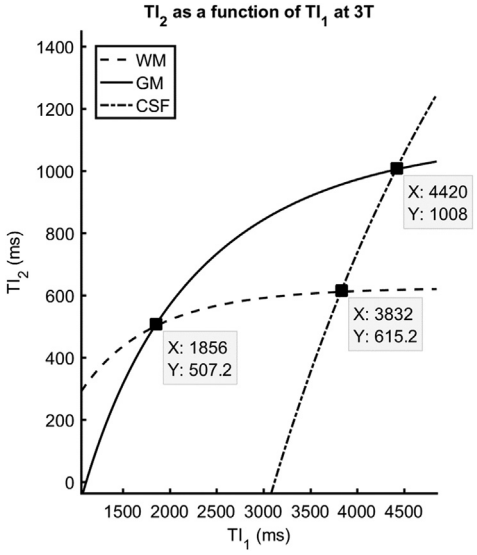

Fig. 6. TI_2 as a function of TI_1 at 3 T for nulling GM, WM and CSF, respectively, each representing the values needed for a single experiment. To create images of just GM, WM or CSF would require three separate scans and would generally take at least 15 min to acquire on a 3 T scanner.

lower region of the brain by the air/tissue interfaces, even for the 7.5 ms echo time, the overall image quality was satisfactory for clinical usage (Table 2). As mentioned earlier, one approach to reducing or eliminating the induced air/tissue susceptibility distortion is to lower the TE from 7.5 ms to 5 ms and/or to reduce slice thickness from 2 mm to 1.34 mm and increase the number of slices. Of course, the latter approach will increase the scan time by 50%.

Representative clinical results in patients with stroke, metastasis and fetal brain with mild ventriculomegaly are shown in Fig. 9, Fig. 10 and Fig. 11, respectively. Representative SWI, FLAIR and tSWI-FLAIR images from a patient with MS demonstrating the central vein sign for WMH lesions are shown in Fig. 12. The latter result is particularly exciting because the SWI and tSWI-FLAIR clearly reveal something new over and above the usual central vein sign, it shows the presence of a vascular abnormality known as a venous angioma (Caput-Medusa) that in itself appears to exactly correlate with the region of inflammation seen in the WMH in the FLAIR data.

4. Discussion

4.1. Potential clinical uses of STAGE

There are a number of neurodegenerative diseases that usually require careful study of tissue properties looking for changes in WM, GM and vascular effects. These include: dementia, multiple sclerosis and stroke as specific examples. Cerebral amyloid angiopathy, hypertension and traumatic brain injury often have microbleeds associated with them. Using STAGE as the standard for structural imaging will always provide T1W imaging, tissue characteristics and SWI for detecting microbleeds. An example of stroke with hypertension is shown in Fig. 9. MRI has been widely utilized for rapid assessment of stroke. [60] For stroke patients, time is brain and for this reason, CT remains the main imaging modality in acute stroke. [41]. Early diagnosis and therapy are very important for improving the prognosis. MR stroke protocols still take on the order of 15 min, which is much longer than CT scanning. [61] In addition, routine MRI is difficult in making accurate and early diagnosis for hemorrhagic stroke, as the components of hematoma vary with time and their imaging manifestations are complicated. [62] However, STAGE not only has the time-shortening advantage for scanning the entire brain in only 5 min, but it also provides SWI and QSM data which are thought to be the most sensitive tools for accurate diagnosis of hemorrhagic stroke and in looking for asymmetrically prominent cortical veins representing changes in deoxyhemoglobin caused by a reduction of tissue perfusion. [63,64] Thus, STAGE can be helpful either in making an accurate and early diagnosis for stroke or if MRI scanning follows the CT scanning it may be able to improve the diagnosis and help better understand patient outcomes.

Contrast enhancement is critical for detecting tumors, tumor boundaries and white matter hyperintensities. Although the T1 images and T1maps provide similar contrast to conventional imaging, the DIR GM images show the tumors particularly well (see Fig. 9). Contrast changes are also seen in the fetal brain, where T1 of WM is now higher than the T1 of GM (see Fig. 10). STAGE offers a means by which to quantify this difference. STAGE SWI can be used to evaluate the fetal brain for oxygen saturation changes and to look for bleeding. Lastly, the use of SWI, QSM and tSWI is particularly useful in Parkinson's disease, where iron content in the substantia nigra is thought to change when the neuromelanin in the nigrosome-1 area depigments [65].

Once the T1 and true PSD maps are obtained, one can simulate a variety of different contrasts and sequences. For example, for a given sequence, it is possible to find the appropriate choice of FA, TR and TE to create the optimal contrast between any two tissues (there is no need to create a large number of images) or for that matter to create an image with no contrast at all (which may have applications such as correcting the RF receive coil field as is currently used in STAGE or in performing fMRI experiments that would then be immune to motion

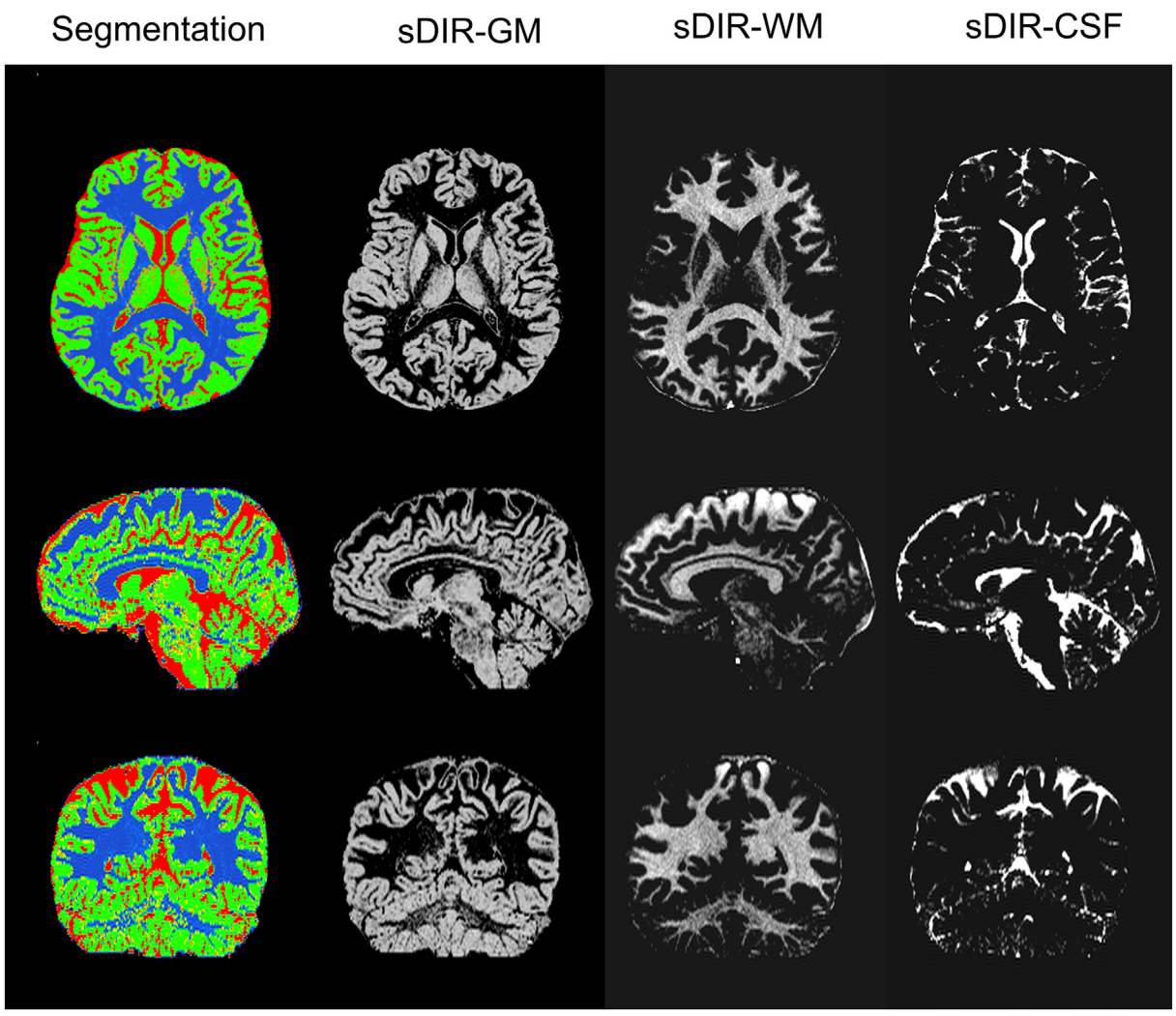

Fig. 7. Representative sDIR images from a STAGE case on a healthy subject. The three sDIR images can be used as naturally segmented data for mapping GM, WM and CSF and potentially for following brain volumes longitudinally in patients.

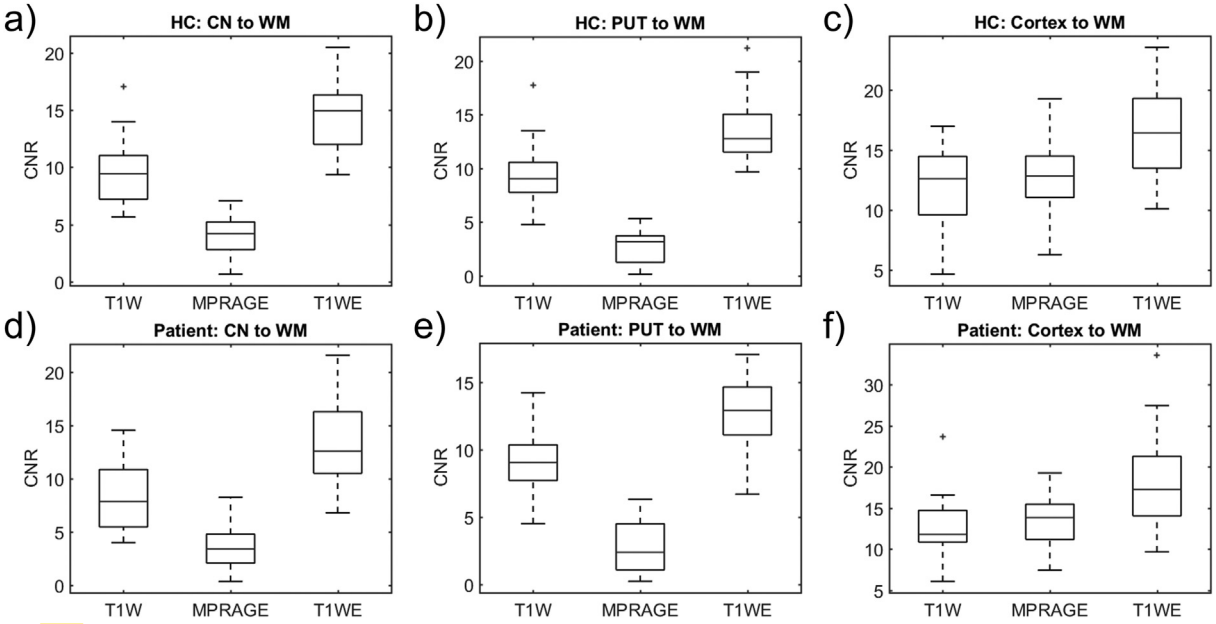

Fig. 8. CNR comparison among conventional T1W from a GRE scan, MPRAGE and STAGE T1WE at 3 T measured over 67 HC and 67 PD patients. Compared to T1W and MPRAGE, STAGE T1WE had significantly improved CNR for CN, PUT and cortex.

Table 2
Overall image quality rating from the three radiologists. Mean ± SD were presented based on all the cases over 67 HC and 67 PD patients.

	T1W	T1WE	T1 map	SWI	tSWI	QSM	MPRAGE
Rater 1	3.9 ± 0.6	4.1 ± 0.5	4.2 ± 0.6	3.9 ± 0.5	3.9 ± 0.5	4.0 ± 0.4	4.0 ± 0.5
Rater 2	4.1 ± 0.7	4.1 ± 0.6	4.2 ± 0.6	4.1 ± 0.5	4.3 ± 0.6	4.1 ± 0.5	4.2 ± 0.6
Rater 3	3.9 ± 0.4	4.0 ± 0.4	4.0 ± 0.3	4.0 ± 0.3	4.0 ± 0.3	3.0 ± 0.2	4.0 ± 0.4

Score criteria: 5 = excellent; 4 = good; 3 = acceptable; 2 = poor; 1 = unacceptable; ≥3 can be used for clinical diagnosis.

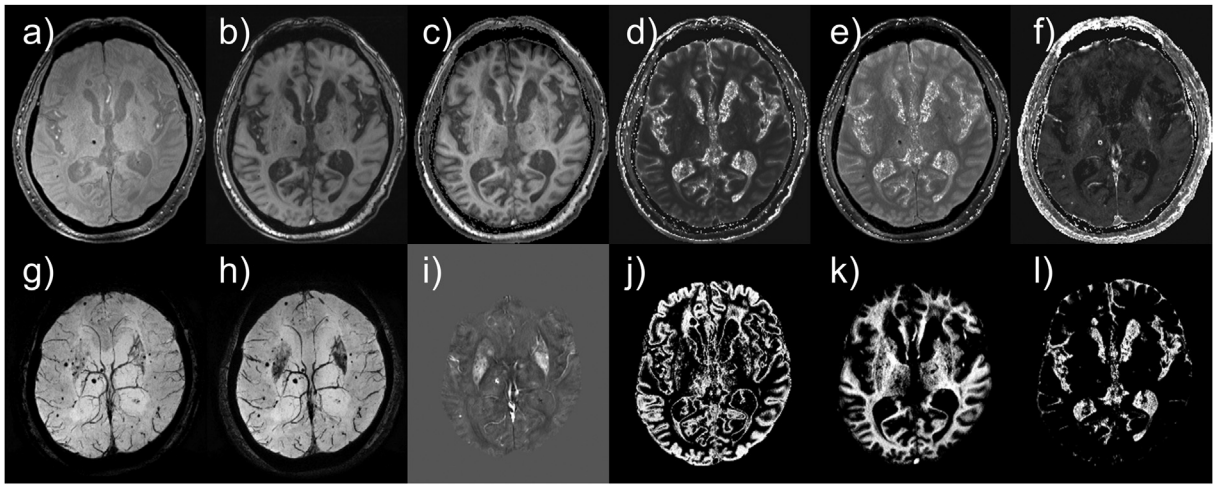

Fig. 9. A stroke case (65Y, male) with cerebral microbleeds scanned with double-echo STAGE on a 3 T scanner. a) PDW; b) T1W; c) T1WE; d) T1 map; e) PSD map; f) R2* map; g) SWI; h) tSWI; i) QSM; j) sDIR-GM; k) sDIR-WM; l) sDIR-CSF. Images g) to i) were maximum/minimum intensity projections giving an effective slice thickness of 16 mm. Note that the cerebral microbleeds appear bright in the R2* map which have similar signal intensity with surrounding tissues on T1WE.

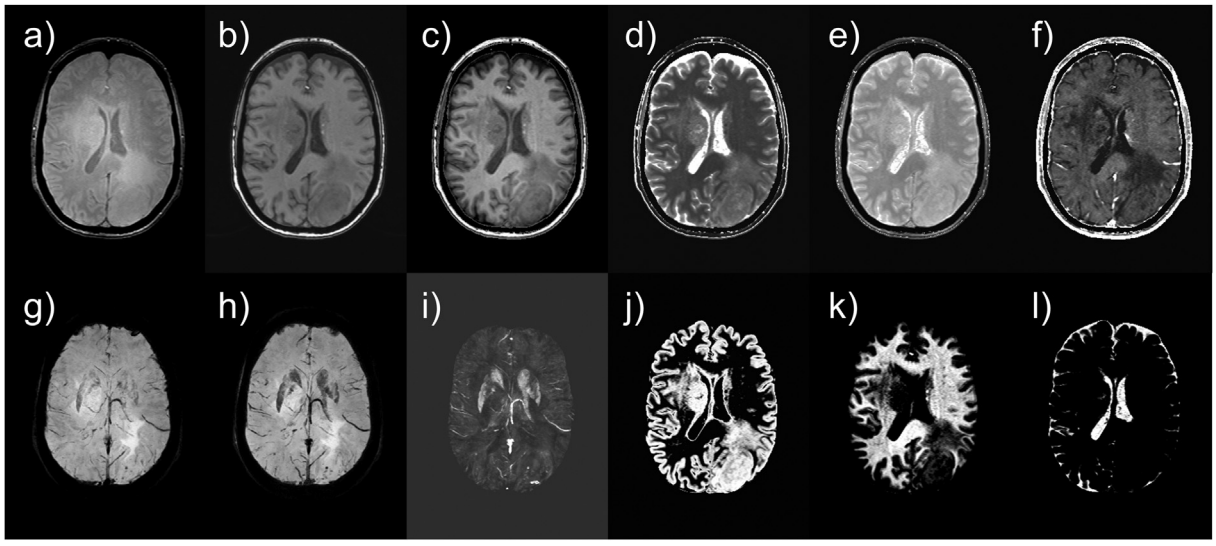

Fig. 10. A metastasis case (62Y, female) scanned with double-echo STAGE on a 3 T scanner. a) PDW; b) T1W; c) T1WE; d) T1 map; e) PSD map; f) R2* map; g) SWI; h) tSWI; i) QSM; j) sDIR-GM; k) sDIR-WM; l) sDIR-CSF. Images g) to i) were maximum/minimum intensity projections giving an effective slice thickness of 16 mm. Note that edema can be seen in the PSD, T1, R2* maps and SWI.

effects since all signals would be the same).

Synthetic MRI (also known as MAGiC [15,16]) offers this capability using 2D spin echo scanning methods in the same time frame as STAGE when run with the same resolution. Fingerprinting is another approach to determine different tissue properties by collecting a set of random k-space coverage with different weightings [12–14]. Once this has been done and estimates of the tissue properties have been obtained it can also be used to simulate different types of image contrast. Currently, fingerprinting requires a longer scan time to acquire the entire brain and has more complicated processing needs compared to STAGE and synthetic MRI [14]. DIR was introduced to null two tissues using two inversion times. [58,66,67] DIR is one of the most sensitive sequences for detecting inflammatory lesions in patients with MS. [68–71] STAGE quantifies T1, PSD and T2* for the entire brain. Therefore, it can provide simulated DIR (sDIR) images for GM, WM and CSF similar to a recently published paper using MAGiC [16].

Finally, STAGE may find applications in other parts of the body such as the breast for detecting cancer, the knee for evaluating cartilage and the lower leg/foot regions for diabetes studies. In each of these cases, a different background tissue will need to be used such as fat for breast

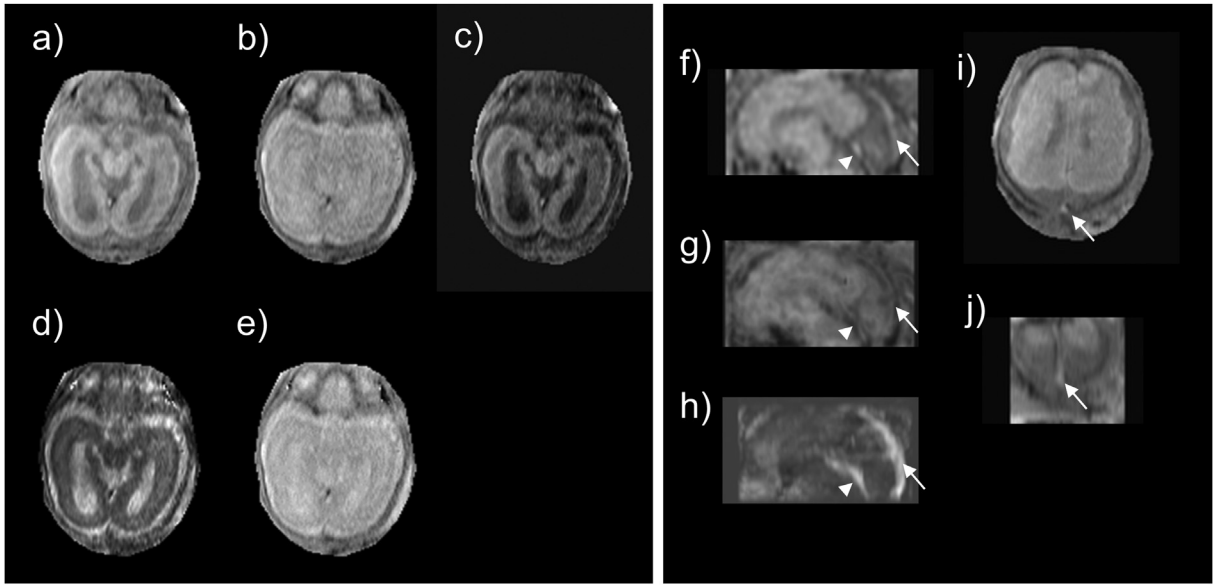

Fig. 11. STAGE for fetal brain imaging (28-week gestational age, ventriculomegaly) using 2D acquisitions. a) T1W (FA = 75°); b) PDW (FA = 15 °); c) T1WE; d) T1 map; e) PSD map; f), i) and j) are T1W images in sagittal view, axial view and coronal view; g) and h) were the minimum/maximum intensity projection of SWI (g) and QSM (h) with effective slice thickness of 15 mm showing the superior sagittal sinus (arrow) and straight sinus (arrow head). Images in this figure were cropped from the original images of the mother.

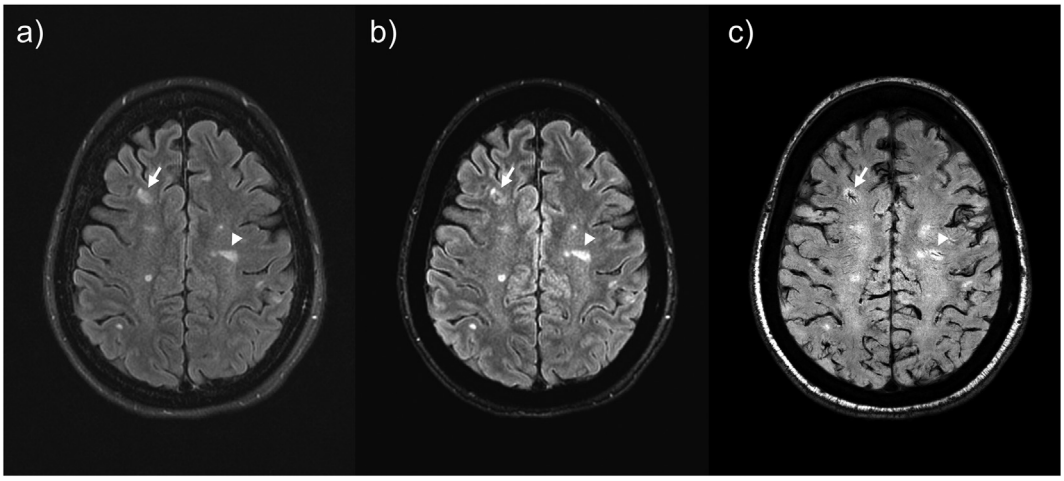

Fig. 12. Representative tSWI-FLAIR in patient with MS. Multiple WMH lesions are shown on the T2 weighted FLAIR (a) data. By combining the tSWI derived from STAGE, the tSWI-FLAIR (b) had suppressed signal at the center of one WMH lesion (arrows). With the presence of an iron-based contrast agent (Ferumoxytol), the contrast enhanced tSWI-FLAIR (c) presented not only the central vein sign (arrow-head) but also a small venous angioma that clearly delineates the region of inflammation (arrow). The use of Ferumoxytol enhanced tSWI-FLAIR could help the study of WMH origins.

imaging and muscle for knee and leg imaging in order to obtain the RF transmit field maps and correct the inherent RF inhomogeneities in the image.

4.2. Limitations

STAGE has several limitations. First, the use of a longer first echo time leads to air/tissue interface problems near the sinuses. This can be alleviated by reducing the echo time to 5 ms keeping flow compensation in the read and slice select directions or by reducing the echo time to 2.5 ms similar to that in MP-RAGE. Second, the lower resolution version does not produce as good an SWI as the usual isotropic in-plane SWI scans. In the future, it may be possible to double the SWI resolution by using a split k-space coverage concept for the second echoes. Third, WM is used as a constraint to find the constant necessary to provide absolute RF transmit field correction. In order to extend STAGE to other parts of the body such as the leg for example, it will be necessary to use the same type of constraint for muscle. This can be done but requires that there is either enough WM in the brain to use as a constraint or enough muscle in the leg to use as a constraint.

5. Conclusions

In the future, it is possible that rather than choosing a specific MR imaging protocol, a method like STAGE will collect all relevant information and radiologists will choose an image review protocol and not an image acquisition protocol because all relevant data they need to make a diagnosis for a given neurodegenerative disease will already be present. In summary, STAGE is a rapid, multi-contrast, protocol that offers: uniform signal across the entire brain, 3D reformattable images for all contrasts and simulated images; gradient echo information including T1W, T1WE, PDW, T2*W, and SWI; as well as quantitative images in the form of QSM, R2* maps, T1 maps and PSD maps.

References

[1] Simon JH, Li D, Traboulsee A, Coyle PK, Arnold DL, Barkhof F, et al. Standardized MR imaging protocol for multiple sclerosis: consortium of MS centers consensus guidelines. Am J Neuroradiol 2006;27:455–61. [doi:27/2/455 [pii].

[2] Packer RA, Rossmeisl JH, Kent MS, Griffin JF, Mazcko C, LeBlanc AK. Consensus recommendations on standardized magnetic resonance imaging protocols for multicenter canine brain tumor clinical trials. Vet Radiol Ultrasound 2018;59:261–71. https://doi.org/10.1111/vru.12608.

[3] Traboulsee A, Simon JH, Stone L, Fisher E, Jones DE, Malhotra A, et al. Revised recommendations of the consortium of MS centers task force for a standardized MRI protocol and clinical guidelines for the diagnosis and follow-up of multiple sclerosis. Am J Neuroradiol 2016;37:394–401. https://doi.org/10.3174/ajnr.A4539.

[4] Ellingson BM, Bendszus M, Boxerman J, Barboriak D, Erickson BJ, Smits M, et al. Consensus recommendations for a standardized brain tumor imaging protocol in clinical trials. Neuro Oncol 2015;17:1188–98. https://doi.org/10.1093/neuonc/nov095.

[5] De Graaf P, Göricke S, Rodjan F, Galluzzi P, Maeder P, Castelijns JA, et al. Guidelines for imaging retinoblastoma: imaging principles and MRI standardization. Pediatr Radiol 2012;42:2–14. https://doi.org/10.1007/s00247-011-2201-5.

[6] Jack CR, Bernstein MA, Fox NC, Thompson P, Alexander G, Harvey D, et al. The Alzheimer's Disease Neuroimaging Initiative (ADNI): MRI methods. J Magn Reson Imaging 2008;27:685–91. https://doi.org/10.1002/jmri.21049.

[7] Brickman AM, Tosto G, Gutierrez J, Andrews H, Gu Y, Narkhede A, et al. An MRI measure of degenerative and cerebrovascular pathology in Alzheimer disease. Neurology 2018. https://doi.org/10.1212/WNL.0000000000006310. 10.1212/WNL.0000000000006310.

[8] Rovira À, Wattjes MP, Tintoré M, Tur C, Yousry TA, Sormani MP, et al. MAGNIMS consensus guidelines on the use of MRI in multiple sclerosis—clinical implementation in the diagnostic process. Nat Rev Neurol 2015;11:471–82. https://doi.org/10.1038/nrneurol.2015.106.

[9] Filippi M, Rocca MA, Ciccarelli O, De Stefano N, Evangelou N, Kappos L, et al. MRI criteria for the diagnosis of multiple sclerosis: MAGNIMS consensus guidelines. Lancet Neurol 2016;15:292–303.

[10] Jauch EC, Saver JL, Adams HP, Bruno A, Connors JJB, Demaerschalk BM, et al. Guidelines for the early management of patients with acute ischemic stroke. Am Hear Assoc Am Stroke Assoc 2013;44:870–947. https://doi.org/10.1161/01.STR.0000163257.66207.2d.

[11] Fiebach JB, Schellinger PD, Gass A, Kucinski T, Siebler M, Villringer A, et al. Stroke magnetic resonance imaging is accurate in hyperacute intracerebral hemorrhage: a multicenter study on the validity of stroke imaging. Stroke 2004;35:502–6. https://doi.org/10.1161/01.STR.0000114203.75678.88.

[12] Ma D, Gulani V, Seiberlich N, Liu K, Sunshine JL, Duerk JL, et al. Magnetic resonance fingerprinting. Nature 2013;495:187–92.

[13] Jiang Y, Ma D, Seiberlich N, Gulani V, Griswold MA. MR fingerprinting using fast imaging with steady state precession (FISP) with spiral readout. Magn Reson Med 2015;74:1621–31.

[14] Bipin Mehta B, Coppo S, Frances McGivney D, Ian Hamilton J, Chen Y, Jiang Y, et al. Magnetic resonance fingerprinting: a technical review. Magn Reson Med 2018. https://doi.org/10.1002/mrm.27403.

[15] Warntjes JBM, Leinhard OD, West J, Lundberg P. Rapid magnetic resonance quantification on the brain: optimization for clinical usage. Magn Reson Med 2008;60:320–9.

[16] Tanenbaum LN, Tsiouris AJ, Johnson AN, Naidich TP, DeLano MC, Melhem ER, et al. Synthetic MRI for clinical neuroimaging: results of the magnetic resonance image compilation (MAGiC) prospective, multicenter, multireader trial. Am J Neuroradiol 2017;38:1103–10. https://doi.org/10.3174/ajnr.A5227.

[17] Hagiwara A, Warntjes M, Hori M, Andica C, Nakazawa M, Kumamaru KK, et al. SyMRI of the brain: rapid quantification of relaxation rates and proton density, with synthetic MRI, automatic brain segmentation, and myelin measurement. Invest Radiol 2017;52:647–57. https://doi.org/10.1097/RLI.0000000000000365.

[18] Chen Y, Liu S, Wang Y, Kang Y, Haacke EM. STrategically Acquired Gradient Echo (STAGE) imaging, part I: creating enhanced T1 contrast and standardized susceptibility weighted imaging and quantitative susceptibility mapping. Magn Reson Imaging 2018;46:130–9. https://doi.org/10.1016/j.mri.2017.10.005.

[19] Wang Y, Chen Y, Wu D, Wang Y, Sethi SK, Yang G, et al. STrategically acquired gradient Echo (STAGE) imaging, part II: correcting for RF inhomogeneities in estimating T1 and proton density. Magn Reson Imaging 2018;46:140–50. https://doi.org/10.1016/j.mri.2017.10.006.

[20] Chen Y, Lagana M, Xia S, Haacke EM. Strategically Acquired Gradient Echo (STAGE) imaging for standardized multi-contrast and quantitative brain data acquisition: Validating T1 mapping and preliminary clinical results. Proc. Intl. Soc. mag. Reson. Med. 27th, Montreal, CA. 2019. p. p1040.

[21] Qu F, Sun T, Chen Y, Yadav B, Jiang L, Qian Z, et al. Fetal brain tissue characterization at 1.5T using STAGE. Proc. Intl. Soc. mag. Reson. Med. 27th., Montreal, CA. 2019. p. p4071.

[22] Horowitz AL, Kaplan RD, Grewe G, White RT, Salberg LM. The ovoid lesion: a new MR observation in patients with multiple sclerosis. Am J Neuroradiol 1989;10:303–5.

[23] Polman CH, Reingold SC, Banwell B, Clanet M, Cohen JA, Filippi M, et al. Diagnostic criteria for multiple sclerosis: 2010 revisions to the McDonald criteria. Ann Neurol 2011. https://doi.org/10.1002/ana.22366.

[24] Obermeier B, Daneman R, Ransohoff RM. Development, maintenance and disruption of the blood-brain barrier. Nat Med 2013. https://doi.org/10.1038/nm.3407.

[25] Minagar A, Alexander JS. Blood-brain barrier disruption in multiple sclerosis. Mult Scler 2003. https://doi.org/10.1191/1352458503ms965oa.

[26] Maggi P, Absinta M, Grammatico M, Vuolo L, Emmi G, Carlucci G, et al. Central vein sign differentiates multiple sclerosis from central nervous system inflammatory vasculopathies. Ann Neurol 2018. https://doi.org/10.1002/ana.25146.

[27] Öztoprak B, Öztoprak I, Yildiz K. The effect of venous anatomy on the morphology of multiple sclerosis lesions: a susceptibility-weighted imaging study. Clin Radiol 2016. https://doi.org/10.1016/j.crad.2016.02.005.

[28] Samaraweera APR, Clarke MA, Whitehead A, Falah Y, Driver ID, Dineen RA, et al. The central vein sign in multiple sclerosis lesions is present irrespective of the T2* sequence at 3 T. J Neuroimaging 2017. https://doi.org/10.1111/jon.12367.

[29] Samaraweera APR, Falah Y, Pitiot A, Dineen RA, Morgan PS, Evangelou N. The MRI central vein marker; differentiating PPMS from RRMS and ischemic SVD. Neurol Neuroimmunol NeuroInflammation 2018. https://doi.org/10.1212/NXI.0000000000000496.

[30] Campion T, Smith RJP, Altmann DR, Brito GC, Turner BP, Evanson J, et al. FLAIR* to visualize veins in white matter lesions: a new tool for the diagnosis of multiple sclerosis? Eur Radiol 2017. https://doi.org/10.1007/s00330-017-4822-z.

[31] Kilsdonk ID, Wattjes MP, Lopez-Soriano A, Kuijer JPA, De Jong MC, De Graaf WL, et al. Improved differentiation between MS and vascular brain lesions using FLAIR* at 7 tesla. Eur Radiol 2014. https://doi.org/10.1007/s00330-013-3080-y.

[32] Kilsdonk ID, Lopez-Soriano A, Kuijer JPA, De Graaf WL, Castelijns JA, Polman CH, et al. Morphological features of MS lesions on FLAIR at 7 T and their relation to patient characteristics. J Neurol 2014. https://doi.org/10.1007/s00415-014-7351-6.

[33] Sati P, George IC, Shea CD, Gaitán MI, Reich DS. FLAIR*: a combined MR contrast technique for visualizing white matter lesions and parenchymal veins. Radiology 2012. https://doi.org/10.1148/radiol.12120208.

[34] Kaunzner UW, Kang Y, Zhang S, Morris E, Yao Y, Pandya S, et al. Quantitative susceptibility mapping identifies inflammation in a subset of chronic multiple sclerosis lesions. Brain 2019. https://doi.org/10.1093/brain/awy296.

[35] Dal-Bianco A, Grabner G, Kronnerwetter C, Weber M, Höftberger R, Berger T, et al. Slow expansion of multiple sclerosis iron rim lesions: pathology and 7 T magnetic resonance imaging. Acta Neuropathol 2017. https://doi.org/10.1007/s00401-016-1636-z.

[36] Gabr RE, Pednekar AS, Kamali A, Lincoln JA, Nelson FM, Wolinsky JS, et al. Interleaved susceptibility-weighted and FLAIR MRI for imaging lesion-penetrating veins in multiple sclerosis. Magn Reson Med 2018. https://doi.org/10.1002/mrm.27091.

[37] Grabner G, Dal-Bianco A, Schernthaner M, Vass K, Lassmann H, Trattnig S. Analysis of multiple sclerosis lesions using a fusion of 3.0 T FLAIR and 7.0 T SWI phase: FLAIR SWI. J Magn Reson Imaging 2011. https://doi.org/10.1002/jmri.22452.

[38] Venkatesan R, Lin W, Haacke EM. Accurate determination of spin-density and T1 in the presence of RF-field inhomogeneities and flip-angle miscalibration. Magn Reson Med 1998;40:592–602. https://doi.org/10.1002/mrm.1910400412.

[39] Haacke EM, Brown RW, Thompson MR, Venkatesan R. Magnetic resonance imaging: physical principles and sequence design. 1st ed New York: Wiley-Liss; 1999.

[40] Deoni SCL, Rutt BK, Peters TM. Rapid combined T1 and T2 mapping using gradient recalled acquisition in the steady state. Magn Reson Med 2003;49:515–26.

[41] Deoni SCL, Peters TM, Rutt BK. High-resolution T1 and T2 mapping of the brain in a clinically acceptable time with DESPOT1 and DESPOT2. Magn Reson Med 2005;53:237–41.

[42] Baudrexel S, Reitz SC, Hof S, Gracien R, Fleischer V, Zimmermann H, et al. Quantitative T1 and proton density mapping with direct calculation of radiofrequency coil transmit and receive profiles from two-point variable flip angle data. NMR Biomed 2016;29:349–60.

[43] Wu D, Liu S, Buch S, Ye Y, Dai Y, Haacke EM. A fully flow-compensated multiecho susceptibility-weighted imaging sequence: the effects of acceleration and background field on flow compensation. Magn Reson Med 2016;76:478–89. https://doi.org/10.1002/mrm.25878.

[44] Feng W, Neelavalli J, Haacke EM. Catalytic multiecho phase unwrapping scheme (CAMPUS) in multiecho gradient echo imaging: removing phase wraps on a voxel-by-voxel basis. Magn Reson Med 2013;70:117–26. https://doi.org/10.1002/mrm.24457.

[45] Chen Y, Liu S, Kang Y, Haacke EM. A rapid, robust multi-echo phase unwrapping method for quantitative susceptibility mapping (QSM) using strategically acquired gradient echo (STAGE) data acquisition. SPIE med. Imaging 2018, SPIE medical imaging 2018. p. 105732U. https://doi.org/10.1117/12.2292951.

[46] Gupta RK. A new look at the method of variable nutation angle for the measurement of spin-lattice relaxation times using fourier transform NMR. J Magn Reson 1977;25:231–5. https://doi.org/10.1016/0022-2364(77)90138-X.

[47] Sacolick LI, Wiesinger F, Hancu I, Vogel MW. B1 mapping by {Bloch}-{Siegert} shift. Magn Reson Med 2010;63:1315–22. https://doi.org/10.1002/mrm.22357.

[48] Morrell GR. A phase-sensitive method of flip angle mapping. Magn Reson Med 2008;60:889–94. https://doi.org/10.1002/mrm.21729.

[49] Hornak JP, Szumowski J, Bryant RG. Magnetic field mapping. Magn Reson Med 1988;6:158–63. https://doi.org/10.1002/mrm.1910060204.

[50] Cunningham CH, Pauly JM, Nayak KS. Saturated double-angle method for rapid B1+ mapping. Magn Reson Med 2006;55:1326–33. https://doi.org/10.1002/mrm.20896.

[51] Dowell NG, Tofts PS. Fast, accurate, and precise mapping of the RF field in vivo using the 180° signal null. Magn Reson Med 2007;58:622–30. https://doi.org/10.1002/mrm.21368.

[52] Chung S, Kim D, Breton E, Axel L. Rapid B1+ mapping using a preconditioning RF pulse with turboFLASH readout. Magn Reson Med 2010;64:439–46. https://doi.org/10.1002/mrm.22423.

[53] Yarnykh VL. Actual flip-angle imaging in the pulsed steady state: a method for rapid

three-dimensional mapping of the transmitted radiofrequency field. Magn Reson Med 2007;57:192–200.
[54] Patenaude B, Smith SM, Kennedy DN, Jenkinson M. A Bayesian model of shape and appearance for subcortical brain segmentation. Neuroimage 2011;56:907–22. https://doi.org/10.1016/j.neuroimage.2011.02.046.
[55] Smith SM, Zhang Y, Jenkinson M, Chen J, Matthews PM, Federico A, et al. Accurate, robust, and automated longitudinal and cross-sectional brain change analysis. Neuroimage 2002;17:479–89. https://doi.org/10.1006/nimg.2002.1040.
[56] Smith SM. Fast robust automated brain extraction. Hum Brain Mapp 2002;17:143–55. https://doi.org/10.1002/hbm.10062.
[57] Manfredonia F, Ciccarelli O, Khaleeli Z, Tozer DJ, Sastre-Garriga J, Miller DH, et al. Normal-appearing brain T1 relaxation time predicts disability in early primary progressive multiple sclerosis. Arch Neurol 2007;64:411–5. https://doi.org/10.1001/archneur.64.3.411.
[58] Redpath TW, Smith FW. Technical note: use of a double inversion recovery pulse sequence to image selectively grey or white brain matter. Br J Radiol 1994;67:1258–63. https://doi.org/10.1259/0007-1285-67-804-1258.
[59] Weiskopf N, Suckling J, Williams G, Correia MMM, Inkster B, Tait R, et al. Quantitative multi-parameter mapping of R1, PD*, MT, and R2* at 3T: a multi-center validation. Front Neurosci 2013. https://doi.org/10.3389/fnins.2013.00095.
[60] van Beek EJR, Kuhl C, Anzai Y, Desmond P, Ehman RL, Gong Q, et al. Value of MRI in medicine: more than just another test? J Magn Reson Imaging 2018. https://doi.org/10.1002/jmri.26211.
[61] Sunshine JL, Tarr RW, Lanzieri CF, Landis DMD, Selman WR, Lewin JS. Hyperacute stroke: ultrafast MR imaging to triage patients prior to therapy. Radiology 1999;212:325–32. https://doi.org/10.1148/radiology.212.2.r99au52325.
[62] Ma X, Bai Y, Lin Y, Hong X, Liu T, Ma L, et al. Amide proton transfer magnetic resonance imaging in detecting intracranial hemorrhage at different stages: a comparative study with susceptibility weighted imaging. Sci Rep 2017;7. https://doi.org/10.1038/srep45696.
[63] Rastogi R, Ding Y, Xia S, Wang M, Luo Y, Choi HS, et al. Recent advances in magnetic resonance imaging for stroke diagnosis. Brain Circ 2015;1:26–37.
[64] Xia S, Utriainen D, Tang J, Kou Z, Zheng G, Wang X, et al. Decreased oxygen saturation in asymmetrically prominent cortical veins in patients with cerebral ischemic stroke. Magn Reson Imaging 2014;32:1272–6. https://doi.org/10.1016/j.mri.2014.08.012.
[65] Lotfipour AK, Wharton S, Schwarz ST, Gontu V, Schäfer A, Peters AM, et al. High resolution magnetic susceptibility mapping of the substantia nigra in Parkinson's disease. J Magn Reson Imaging 2012. https://doi.org/10.1002/jmri.22752.
[66] Bydder GM. MR imaging: clinical use of the inversion recovery sequence. J Comput Assist Tomogr 1985. https://doi.org/10.1097/00004728-198507010-00002.
[67] Young IR, Hall AS, Bydder GM. The design of a multiple inversion recovery sequence for T1 measurement. Magn Reson Med 1987;5:99–108. https://doi.org/10.1002/mrm.1910050202.
[68] Geurts JJG, Pouwels PJW, Uitdehaag BMJ, Polman CH, Barkhof F, Castelijns JA. Intracortical lesions in multiple sclerosis: improved detection with 3D double inversion-recovery MR imaging. Radiology 2005;236:254–60. https://doi.org/10.1148/radiol.2361040450.
[69] Calabrese M, De Stefano N, Atzori M, Bernardi V, Mattisi I, Barachino L, et al. Detection of cortical inflammatory lesions by double inversion recovery magnetic resonance imaging in patients with multiple sclerosis. Arch Neurol 2007;64:1416–22. https://doi.org/10.1001/archneur.64.10.1416.
[70] Geurts JJG, Roosendaal SD, Calabrese M, Ciccarelli O, Agosta F, Chard DT, et al. Consensus recommendations for MS cortical lesion scoring using double inversion recovery MRI. Neurology 2011;76:418–24. https://doi.org/10.1212/WNL.0b013e31820a0cc4.
[71] Hagiwara A, Hori M, Yokoyama K, Takemura MY, Andica C, Tabata T, et al. Synthetic MRI in the detection of multiple sclerosis plaques. Am J Neuroradiol 2017;38:257–63. https://doi.org/10.3174/ajnr.A5012.